

# Configuration interaction in symmetry-conserving covariant density functional theory

P. W. Zhao,<sup>1,2</sup> P. Ring,<sup>3,2</sup> and J. Meng<sup>2,4</sup>

<sup>1</sup>*Physics Division, Argonne National Laboratory, Argonne, Illinois 60439, USA*

<sup>2</sup>*State Key Laboratory of Nuclear Physics and Technology,  
School of Physics, Peking University, Beijing 100871, China*

<sup>3</sup>*Physik Department, Technische Universität München, D-85747 Garching, Germany*

<sup>4</sup>*School of Physics and Nuclear Energy Engineering, Beihang University, Beijing 100191, China*

A new method to calculate spectroscopic properties of deformed nuclei is proposed: configuration interaction on top of projected density functional theory (CI-PDFT). The general concept of this approach is discussed in the framework of covariant density functional theory and its validity is illustrated in an application to the yrast band of the nucleus  $^{54}\text{Cr}$ . It is found that the experimentally observed excitation energies for the yrast band in  $^{54}\text{Cr}$  can be well reproduced. In contrast to conventional shell-model calculations, there is no core and only a relatively small number of configurations is sufficient for a satisfying description. No new parameters are necessary, because the effective interaction is derived from an universal density functional given in the literature.

PACS numbers: 21.60.Jz, 21.10.Re, 23.20.-g, 27.40.+z

Configuration interaction shell models [1] as well as energy density functional theories (DFTs) [2, 3] have been widely applied in the literature to the description of nuclear properties. The shell model has the advantage of allowing the description of all the spectroscopic properties of the system in the laboratory frame. The physics contained in this approach is mainly expressed in terms of strong mixing between different configurations, while a single configuration contains little physics. The configuration mixing is determined by effective interactions, which strongly depend on the choice of active shells and various truncation schemes. Therefore, no universal shell-model interaction can be used for all nuclei. Moreover, in order to preserve rotational symmetry connected with the quantum numbers of angular momentum, most of these calculations are carried out in a spherical basis. Within this scheme, calculations for heavy deformed nuclei usually have to be carried out in large valence spaces and, as a consequence, the dimensions of the corresponding matrices are huge. This limits most of the applications of the shell-model approach for heavy nuclei to spherical or nearly spherical systems.

Nuclear energy DFT has played an important role in the self-consistent description of nuclei. In contrast to the configuration interaction shell model, DFT is applicable for nuclei all over the nuclide chart as the complicated many-body problem is mapped onto a single-particle problem, which is relatively easy to solve. Over the years, several universal energy density functionals have been constructed, providing a successful description with only a few phenomenological parameters. They describe fruitful physics around the minima of the energy surfaces, and correlations are taken into account by breaking the essential symmetries. The disadvantage of this method is that, in the first place, it is limited to nuclear ground states, and that many spectroscopic properties are not accessible within this approach.

It is clear that the shell model and DFT are really two complementary theoretical strategies to understand

nuclear structure. Nuclear DFT is applicable for the description of ground states and of bulk properties of almost all nuclei in the nuclear chart, while shell-model calculations reproduce fully quantum mechanically the spectroscopic details in specific regions of the periodic table. Therefore, for the goal of a unified and comprehensive description of all nuclei, it is essential to develop a theory which combines the advantages from both approaches.

In the DFT regime, the generator coordinate method (GCM) has been used to go beyond mean field and to study additional correlations [2, 4]. This approach has been implemented in the nonrelativistic Skyrme [5, 6] and Gogny [7] functionals, and also the relativistic functionals [8, 9]. Further developments considering the triaxial and the octupole degrees of freedom are also available for both the nonrelativistic [10–12] and relativistic [13–16] models. Using the Gaussian overlap approximation (GOA), it can be considerably simplified through the derivation of a collective Hamiltonian, which is relatively simple for heavy systems. This method has been applied in Refs. [17–19] with nonrelativistic functionals and Refs. [20–22] with relativistic ones. However, all these methods are limited to the description of very specific types of excitations (e.g., to quadrupole and/or octupole modes) and they can be applied only for relatively low energies, i.e., below the first two-quasiparticle excitations [4].

For high-spin spectra, the cranking model [23] has proven to be very practical and successful as it is a first-order approximation for a variation after projection onto good angular momentum [24]. Cranking models based on the DFTs have been widely used with the nonrelativistic functionals [25, 26] and the relativistic ones [27–29]. Moreover, the tilted axis cranking relativistic Hartree [30–32] and Hartree-Bogoliubov models [33] have been developed and have achieved great success in many novel rotational bands [34–36]. Similar approaches are also available with the nonrelativistic

tic functionals [37, 38]. However, the cranking models describe the physics only on average in a rotating mean field. They mix configurations at constant angular velocity and not at constant angular momentum. Therefore, level crossing phenomena are not described properly [39]. Attempts to include correlations due to symmetry breaking [40] and to mix configuration beyond the rotating mean field [41] are still in their infancy.

Therefore, we propose here a method which allows us to include quasiparticle excitations, i.e., to mix collective and multiparticle excitations. We call it configuration interaction-projected density functional theory (CI-PDFT). In such a theory, we start from a successful density functional, and the self-consistent solution gives rise to a state in a minimum of the energy surface. This state contains already important physics, and additional correlations, as required for spectroscopic studies, can be taken into account with shell-model calculations in a configuration space built on top of the minimum state from DFT. The dimension of such a configuration space can be much smaller than that of a traditional shell-model calculation for heavy nuclei, because the basis is not arbitrary, but optimized to the ground state. The DFT solutions used here contain already important correlations. Therefore, one can hope that such a method will be able in the future to provide a global study of many nuclear properties with no additional parameters beyond those of the well-established density functional. Technically, this is reminiscent of the successful phenomenological projected shell model (PSM) based on the Nilsson potential proposed by Hara and Sun [42–44]. This model, however, is limited to a few valence shells. It is based on a pairing-plus-quadrupole interaction and contains several phenomenological parameters, which have to be adjusted in different mass regions. In contrast, DFT is a more fundamental and self-consistent theory based on more realistic two-body interactions.

In principle, this new method is applicable for all kind of density functionals. Here, we concentrate on covariant density functional theory (CDFT), which has achieved great success in describing many nuclear phenomena [3, 34, 45–47]. The CDFT starts from a Lagrangian and the corresponding Kohn-Sham equations derived from this Lagrangian have the form of a Dirac equation with effective fields  $S(\mathbf{r})$  and  $V^\mu(\mathbf{r})$  [48]. They are driven in a self-consistent way by the densities and current distributions. For open-shell nuclei, pairing correlations have to be taken into account. The nuclear ground-state wave function  $|\Phi\rangle$  corresponds to a quasiparticle vacuum, where the quasiparticle basis can be defined by a Bogoliubov transformation of a particle basis. Self-consistent solutions for the single-quasiparticle Kohn-Sham equation yield the ground-state wave function  $|\Phi\rangle$ ; for details, see Refs. [4, 45, 49, 50].

Starting from the ground state obtained in this way, one easily finds many multi-quasiparticle states, and they, together with the ground state, form the configuration space. One has to note that, here, rotational symmetry

is violated for deformed nuclei; i.e., none of the states in the above configuration space is an eigenstate of the angular momentum, and there are no good quantum numbers. This forbids a satisfying description of spectroscopic properties and, thus, angular momentum projection is required for these configurations [51].

Suppose that we have chosen the set  $\{|\Phi_\kappa\rangle\}$  of multi-quasiparticle states; the wave function  $|\Psi\rangle$  in the laboratory frame with good angular momentum quantum numbers  $I$  and  $M$  is obtained by projection. For simplicity, we assume here axial symmetry of the basis; i.e., each of the multi-quasiparticle components  $|\Phi_\kappa\rangle$  is characterized by a quantum number  $K$ , the projection of the angular momentum onto the intrinsic symmetry axis. We thus find

$$|\Psi_{IM}^\alpha\rangle = \sum_{\kappa} F_{\kappa}^{I\alpha} \hat{P}_{MK}^I |\Phi_{\kappa}\rangle. \quad (1)$$

Here,  $\hat{P}_{MK}^I$  is the angular momentum projection operator [51], and the expansion coefficients  $F_{\kappa}^{I\alpha}$  of the eigenstate with the label  $\alpha$  are determined by requiring that the energy expectation value is stationary with respect to an arbitrary variation of  $F_{\kappa}^{I\alpha}$ . This means that the Hamiltonian is diagonalized in the shell-model subspace spanned by the nonorthogonal basis  $\{\hat{P}_{MK}^I |\Phi_{\kappa}\rangle\}$ , and this leads to the generalized eigenvalue equations

$$\sum_{\kappa'} \{H_{\kappa\kappa'}^I - E_{\alpha}^I N_{\kappa\kappa'}^I\} F_{\kappa'}^{I\alpha} = 0, \quad (2)$$

with the Hamiltonian overlap matrix  $H_{\kappa\kappa'}^I$  and the norm overlap matrix  $N_{\kappa\kappa'}^I$ :

$$H_{\kappa\kappa'}^I = \langle \Phi_{\kappa} | \hat{H} \hat{P}_{KK'}^I | \Phi_{\kappa'} \rangle, \quad N_{\kappa\kappa'}^I = \langle \Phi_{\kappa} | \hat{P}_{KK'}^I | \Phi_{\kappa'} \rangle. \quad (3)$$

The weight functions  $F_{\kappa}^{I\alpha}$  are normalized by the condition

$$\sum_{\kappa\kappa'} F_{\kappa}^{I\alpha} N_{\kappa\kappa'}^I F_{\kappa'}^{I\alpha'} = \delta_{\alpha\alpha'}. \quad (4)$$

Here,  $\hat{H}$  represents the residual interaction [51], which, in the present framework of relativistic density functional theory, is found as the second derivative of the energy density functional with respect to the density matrix [52]:

$$V_{nmn'm'} = \frac{\delta^2 E[\hat{\rho}]}{\delta \hat{\rho}_{nm} \delta \hat{\rho}_{n'm'}}. \quad (5)$$

Since the exchange terms are neglected in the mean-field calculations, for self-consistency, we should also neglect exchange terms in the present beyond mean-field level. Moreover, as the first step, we also neglect the contribution from the spacelike components of the vector channel in the present work due to the limitation of numerical costs.

As usual for generalized eigenvalue problems of the form (1), the basis functions  $\hat{P}_{MK}^I |\Phi_{\kappa}\rangle$  are not orthogonal and, therefore, the coefficients  $F_{\kappa}^{I\alpha}$  cannot be interpreted as probability amplitudes for the state  $\kappa$ . As

discussed in Ref. [51], these probability amplitudes  $G_{\kappa}^{I\alpha}$  are written as

$$G_{\kappa}^{I\alpha} = \sum_{\kappa\kappa'} (N^I)_{\kappa\kappa'}^{1/2} F_{\kappa'}^{I\alpha}. \quad (6)$$

Once the weights  $F_{\kappa}^{I\alpha}$  of the nuclear collective wave functions  $|\Psi_{IM}^a\rangle$  in Eq. (1) are known, it is straightforward to calculate all physical observables, such as the electromagnetic transition probabilities. The reduced transition probability for a transition between an initial state  $I_i$  and a final state  $I_f$  is defined by

$$B(E2; I_i, \alpha \rightarrow I_f, \alpha') = \frac{e^2}{2I_i + 1} \left| \langle \Psi_{I_f}^{\alpha'} || \hat{Q}_2 || \Psi_{I_i}^{\alpha} \rangle \right|^2. \quad (7)$$

Note that here  $e$  denotes the bare value of the proton charge, and there is no need to introduce effective charges.

In this paper, the results of the newly developed CI-PDFPT are illustrated by taking the nucleus  $^{54}\text{Cr}$  as an example. In order to simplify the evaluation of the Hamiltonian and the norm overlap, we used the relativistic point coupling Lagrangian PC-PK1 [50]. This avoids the complicated overlap integrals for functionals with finite range. As the first application, the particle number projection is not included. Therefore, we employ an approximate scheme for correcting the mean value of the particle number as in Ref [53]. It has also been found in numerous applications that the simple phenomenological PSM [42] is very successful without particle number projection. The single-nucleon wave functions are solved via an expansion in a basis of cylindrical harmonic oscillator wave functions with  $N_F = 12$  major shells, and the basis parameters are  $\hbar\omega_0 = 41A^{-1/3}$  and  $\beta_0 = 0$  [54, 55]. Pairing correlations are treated by the BCS method with the density-independent  $\delta$  force given in Ref. [50]. We have checked that the oscillator expansion has converged well for  $N_F = 12$ . It is found that the lowest energy state has a prolate deformation of around  $\beta_2 = 0.24$ . This is in agreement with the experimental value  $\beta_2 = 0.247 \pm 0.067$  of Ref. [56].

The evaluation of the Hamiltonian and the norm overlap integrals in Eq. (3) can be carried out in particle space (see, for instance, Ref. [8]) or in quasiparticle space. In this work, we used the latter method following the expressions of Ref. [42] for separable effective interactions. For this purpose, we expressed the interaction terms in the zero-range functional PC-PK1 as a sum of separable terms in a similar way as it has been done in Refs. [52, 57] for the zero-range functionals PC-F1 [58] and DD-PC1 [59].

The neutron and proton single-particle levels are presented in Fig. 1 as functions of the quadrupole deformation  $\beta_2$ . It is important to identify the single-particle states near the Fermi surfaces, which take part in the low-lying quasiparticle excitations. In the present work, the configuration space consists of the zero- and two-quasiparticle states

$$|0\rangle, \quad \alpha_{\nu}^{\dagger} \alpha_{\nu'}^{\dagger} |0\rangle, \quad \alpha_{\pi}^{\dagger} \alpha_{\pi'}^{\dagger} |0\rangle, \quad (8)$$

and the dimension of this configuration space is truncated with an cutoff in the two-quasiparticle excitation energy  $E_{\text{cut}} = 6.5$  MeV for both protons and neutrons. The corresponding configuration space consists of 37 states including 18 two-quasineutron, 18 two-quasiproton excited states, and the quasiparticle vacuum  $|0\rangle$ . The convergence of the dimension of the configuration space has been tested by comparing with the results obtained with a larger energy cutoff  $E_{\text{cut}} = 7.0$  MeV, and it turns out that such a configuration space is sufficient to obtain convergent results for the states with  $I \leq 10$  in  $^{54}\text{Cr}$ .

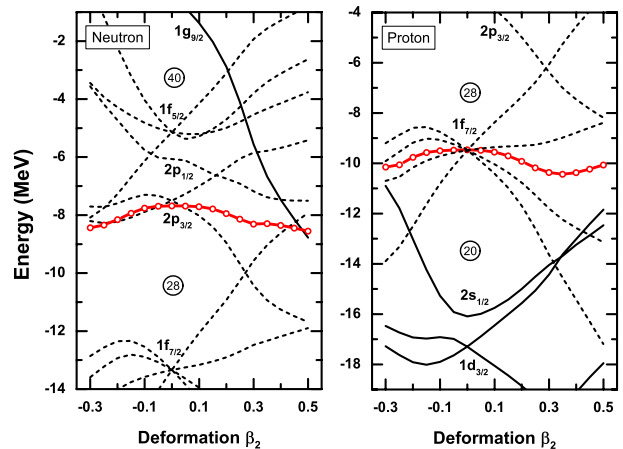


FIG. 1. (Color online) The neutron (left panel) and proton (right panel) single-particle levels for  $^{54}\text{Cr}$ , as functions of the quadrupole deformation  $\beta_2$ . The dashed and solid lines represent the levels with negative and positive parities, respectively. The thick lines with open circles denote the position of the Fermi energy.

In the inset of Fig. 2, the energies of angular momentum projected states for all the 37 configurations contained in the present calculation are shown as functions of the angular momentum together with the yrast band. Such a figure is also called a band diagram [42], in which the rotational behavior of each configuration, as well as its relative energy compared to other configurations, is clearly visualized. Therefore, one has to trace the configuration of each band in the band diagram. Since axial symmetry is imposed in the present work, the  $K$  value (the projection of angular momentum on the symmetry axis of the deformed system) can be easily used to identify the configurations. Note that the angular momentum for each configuration does not always start from zero due to the fact that the starting angular momentum  $I$  should satisfy the relation  $I \geq |K|$ . Moreover, the starting angular momentum for each configuration is also not necessarily equal to the spin of the corresponding band-head, since in some cases, as shown in Fig. 2, the band energies are not always increasing with the spin.

For even-even nuclei, the zero quasiparticle ground band has  $K = 0$ , whereas a two quasiparticle band has a  $K$  given by the coupling of the  $K$  values of its constituent quasiparticles. A superposition of them imposed by con-

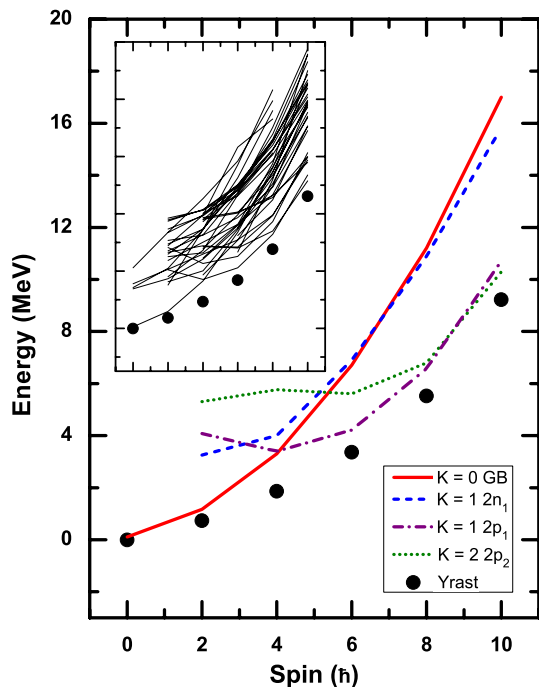


FIG. 2. (Color online) Theoretical yrast band (solid circles) and the angular momentum projected states for some important configurations which are explained in Table I in  $^{54}\text{Cr}$ . Inset: Angular momentum projected states for all the configurations considered together with the yrast band (solid circles). Note that the energy of the yrast state  $0^+$  is renormalized to zero.

figuration mixing gives the final results at each spin. The ensemble of the lowest calculated states with the energy  $E_0^I$  at each spin forms the yrast band, which is shown by solid circles in Fig. 2.

It is usually not necessary to put too many bands in a single band diagram, but to select instead some of the most important ones. In Fig. 2, the theoretical band diagram for some important configurations are given together with the yrast band; these different bands can be distinguished by different line styles. It has been found that, as the nucleus starts rotating, the energy of the ground-state band increases rapidly toward the higher-energy region. However, the two quasiparticle bands rise slowly with spin and, therefore, they can cross the ground-state band. Here, we use  $2n_1$ ,  $2p_1$ , and  $2p_2$  to label the relevant configurations, and the detailed information is listed in Table I.

After configuration mixing by diagonalizing the residual interaction in the projected configuration space, the yrast states are obtained (solid circles in Fig. 2), and these are the theoretical results to be compared with the data. In Fig. 3, the calculated energy levels and the  $B(E2; \downarrow)$  transition probabilities are given in comparison with the available data [60] for the yrast band and also the nonyrast  $I = 2, 4$  states.

In Table I, we show, for each of the yrast states with angular momentum  $I$ , the corresponding decomposition

into the basis configurations. These configurations are characterized by their quasiparticle energies  $E = E_1 + E_2$ , their  $K$  values, and their approximate quantum numbers in the spherical basis. The remaining columns represent the amplitudes  $G_\kappa^I$  of the yrast states in Eq. (6). As expected, it is found that the ground state with  $I = 0$  has only  $K = 0$  admixtures. It corresponds essentially to the mean-field ground state  $|0\rangle$ . With increasing angular momentum, we observe admixtures of higher  $K$  values, in particular of the  $K = 1$  two-neutron state  $2n_1$ , the  $K = 1$  two-proton state  $2p_1$ , and the  $K = 2$  two-proton state  $2p_2$ . This is in agreement with the band diagram in Fig. 2.

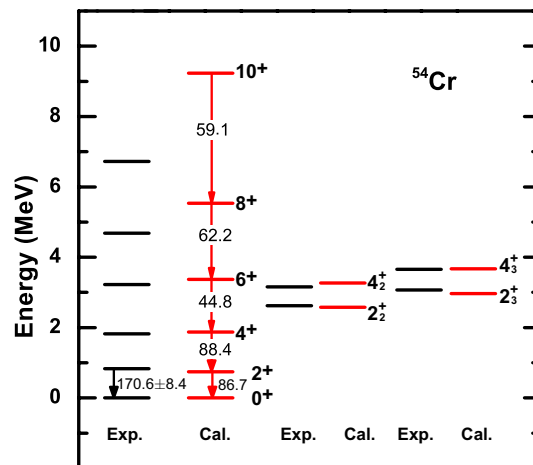


FIG. 3. (Color online) Comparison between the calculated energy levels (MeV) and  $B(E2; \downarrow)$  transition probabilities ( $e^2 \text{fm}^4$ ) and the corresponding data available in Refs. [56, 60] for the yrast band with the angular momentum  $I \leq 10$ , and also the nonyrast  $I = 2, 4$  states.

It is found that the calculated energies for yrast  $I = 2, 4, 6\hbar$  states, and also the nonyrast  $I = 2, 4$  states are in good agreement with the data. However, the calculated  $B(E2; 2^+ \rightarrow 0)$  transition probability is roughly a factor two smaller than the experimental value. This might have to do with the fact that, as seen in Table I, besides the quasiparticle vacuum  $|0\rangle$ , admixtures of 2-neutron configurations mostly contribute to the  $2^+$  state wave function, and these do not contribute to the  $B(E2; 2^+ \rightarrow 0)$  value. For the higher spin states with  $I = 8, 10\hbar$ , the calculated band is too extended in comparison with the data, or in other words, the calculated moments of inertia are too small. The reason for this type of deviation could be the neglect of the time-odd components and, thus, the omission of the mixed currents in the present calculations. In fact, it has been shown that the time-odd components would influence the higher spin states in the previous investigation of rotational bands with cranking CDFT (see, e.g., Refs. [28, 61]). In this context, it was found that the inclusion of time-odd components can increase the moments of inertia and, thus, lead to more compressed rotational bands. On the other

TABLE I. Important configurations with their quasiparticle excitation energies and the amplitudes  $G_{\kappa}^I$  in the yrast state. Here, we list only the configurations whose contributions to the yrast state are larger than 1%.

	$E$	$K$	Configurations	0	2	4	6	8	10
gs	0.00	0	–	0.959	0.856	0.623	0.280	0.150	0.113
$2n1$	2.68	1	$(2p_{3/2})_{k=1/2} \otimes (1f_{5/2})_{k=1/2}$		0.314	0.448	0.241	0.098	0.100
	3.36	1	$(2p_{3/2})_{k=1/2} \otimes (2p_{3/2})_{k=-3/2}$		0.225	0.308	0.164	0.055	0.000
	4.64	2	$(2p_{3/2})_{k=1/2} \otimes (1f_{5/2})_{k=3/2}$		-0.044	-0.146	-0.076	-0.037	-0.064
	4.64	1	$(2p_{3/2})_{k=1/2} \otimes (1f_{5/2})_{k=-3/2}$		0.068	0.126	0.085	0.037	0.028
$2p1$	2.39	0	$(1f_{7/2})_{k=5/2} \otimes (1f_{7/2})_{k=-5/2}$	0.265	0.146	-0.084	-0.232	-0.228	-0.166
	2.55	1	$(1f_{7/2})_{k=3/2} \otimes (1f_{7/2})_{k=-5/2}$		0.224	0.430	0.521	0.400	0.341
	2.55	4	$(1f_{7/2})_{k=3/2} \otimes (1f_{7/2})_{k=5/2}$			0.013	0.205	0.183	0.146
	2.71	0	$(1f_{7/2})_{k=3/2} \otimes (1f_{7/2})_{k=-3/2}$	-0.055	-0.028	0.020	0.283	0.297	0.280
$2p2$	3.56	2	$(1f_{7/2})_{k=1/2} \otimes (1f_{7/2})_{k=-5/2}$		-0.047	-0.127	-0.386	-0.416	-0.409
	3.56	3	$(1f_{7/2})_{k=1/2} \otimes (1f_{7/2})_{k=5/2}$			-0.018	-0.270	-0.320	-0.332
	3.71	1	$(1f_{7/2})_{k=1/2} \otimes (1f_{7/2})_{k=-3/2}$		0.076	0.159	-0.088	-0.277	-0.256
	3.71	2	$(1f_{7/2})_{k=1/2} \otimes (1f_{7/2})_{k=3/2}$		-0.043	-0.075	0.070	0.178	0.152
	4.42	1	$(1f_{7/2})_{k=5/2} \otimes (1f_{7/2})_{k=-7/2}$		-0.152	-0.142	-0.019	0.020	0.061
	4.42	6	$(1f_{7/2})_{k=5/2} \otimes (1f_{7/2})_{k=7/2}$				-0.130	-0.069	-0.054
	4.57	2	$(1f_{7/2})_{k=3/2} \otimes (1f_{7/2})_{k=-7/2}$		0.009	-0.073	-0.180	-0.204	-0.227
	4.57	5	$(1f_{7/2})_{k=3/2} \otimes (1f_{7/2})_{k=7/2}$				0.194	0.216	0.192
	5.58	3	$(1f_{7/2})_{k=1/2} \otimes (1f_{7/2})_{k=-7/2}$			0.032	0.148	0.286	0.367
	5.58	4	$(1f_{7/2})_{k=1/2} \otimes (1f_{7/2})_{k=7/2}$			-0.002	-0.152	-0.251	-0.355

hand, it is possible that the influence of four-quasiparticle configurations should be taken into account. In fact, investigations within the phenomenological projected shell model in this region of the periodic table [44], which include also four-quasiparticle configurations, exhibit better agreement with the experimental data, but at the cost of phenomenological parameters. In order to answer such questions, more detailed investigations within CI-PDFT are definitely necessary.

We proposed a new method, called CI-PDFT, for the description of spectra of deformed nuclei all over the periodic table. Starting from a successful density functional, a minimum in the energy surface is found and a number of quasiparticle configurations is determined. Together with the deformed ground state, they are projected to restore the symmetries broken at the mean field level, and these projected states form the space for configuration mixing calculations using the effective interaction derived from the underlying energy density functional. In this way, one keeps all the advantages of the mean field theory, and goes beyond mean field through mixing of states with good symmetries, which is a concept of the standard shell model. This method will provide a tool for a global study of many nuclear properties with no parameters beyond those of the well-established underlying density functional.

A computer code was developed for relativistic point coupling models and first calculations have been carried out for the Lagrangian PC-PK1. Pairing correlations are taken into account with a  $\delta$  force. The method has been tested for the  $^{54}\text{Cr}$  nucleus. It has been found that the ground state has a quadrupole deformation  $\beta_2 = 0.24$ . By using this minimum as a basis for the projection and after configuration mixing by diagonalizing the residual interaction in a sufficient projected configuration space,

the experimental yrast band in  $^{54}\text{Cr}$  can be reproduced in the low spin part of the band, while the calculated band is too extended for the high-spin part. The present investigation is quite simple. It can be improved in several ways: The effects of time-odd components in the residual interaction should be considered carefully and higher configurations with more quasiparticles could be included. The present model also cannot describe collective vibrations. In principle, this is possible by considering a larger number of two-quasiparticle states in the basis. Work in this direction is in progress.

We note that our model may also be used to describe the mixing of different shapes and shape coexistence phenomena, if the shapes are just obtained by a reoccupation of two particles, as it happens in many light nuclei. A more detailed investigation along this direction is required in the future. Moreover, if one considers only the band heads of collective bands, e.g.,  $\gamma$  bands, the quasiparticle random phase approximation (QRPA) will be certainly a much simpler model, and it would be interesting to compare QRPA with our method. However, the QRPA approaches based on a fixed minimum will not be able to describe collective high-spin states, for which one would need QRPA based on cranked mean-field states (see, e.g., Ref. [62]).

## ACKNOWLEDGMENTS

We thank R. V. F. Janssens and Robert B. Wiringa for careful reading of the manuscript. This work is supported by U.S. Department of Energy (DOE), Office of Science, Office of Nuclear Physics, under Contract No. DE-AC02-06CH11357, by the Chinese Major State 973 Program 2013CB834400, and by the NSFC Grant No.

11335002 and No. 11621131001. We also acknowledge support from the Laboratory Computing Resource Cen-

ter at Argonne National Laboratory, and the DFG Cluster of Excellence “Origin and Structure of the Universe” ([www.universe-cluster.de](http://www.universe-cluster.de)).

- 
- [1] E. Caurier, G. Martínez-Pinedo, F. Novacki, A. Poves, and A. P. Zuker, *Rev. Mod. Phys.* **77**, 427 (2005).
- [2] M. Bender, P.-H. Heenen, and P.-G. Reinhard, *Rev. Mod. Phys.* **75**, 121 (2003).
- [3] in *Relativistic Density Functional for Nuclear Structure*, International Review of Nuclear Physics, Vol. 10, edited by J. Meng (World Scientific, Singapore, 2016).
- [4] T. Nikšić, D. Vretenar, and P. Ring, *Prog. Part. Nucl. Phys.* **66**, 519 (2011).
- [5] A. Valor, P.-H. Heenen, and P. Bonche, *Nucl. Phys. A* **671**, 145 (2000).
- [6] M. Bender, G. F. Bertsch, and P. H. Heenen, *Phys. Rev. C* **73**, 034322 (2006).
- [7] R. Rodríguez-Guzmán, J. L. Egidio, and L. M. Robledo, *Nucl. Phys. A* **709**, 201 (2002).
- [8] T. Nikšić, D. Vretenar, and P. Ring, *Phys. Rev. C* **73**, 034308 (2006).
- [9] T. Nikšić, D. Vretenar, and P. Ring, *Phys. Rev. C* **74**, 064309 (2006).
- [10] M. Bender and P.-H. Heenen, *Phys. Rev. C* **78**, 024309 (2008).
- [11] T. R. Rodríguez and J. L. Egidio, *Phys. Rev. C* **81**, 064323 (2010).
- [12] R. Rodríguez-Guzmán, L. M. Robledo, and P. Sarriguren, *Phys. Rev. C* **86**, 034336 (2012).
- [13] J. M. Yao, E. F. Zhou, and Z. P. Li, *Phys. Rev. C* **92**, 041304 (2015).
- [14] E.-F. Zhou, J. Yao, Z. Li, J. Meng, and P. Ring, *Phys. Lett. B* **753**, 227231 (2016).
- [15] J. M. Yao, J. Meng, P. Ring, and D. P. Arteaga, *Phys. Rev. C* **79**, 044312 (2009).
- [16] J. M. Yao, J. Meng, P. Ring, and D. Vretenar, *Phys. Rev. C* **81**, 044311 (2010).
- [17] J. Libert, M. Girod, and J.-P. Delaroche, *Phys. Rev. C* **60**, 054301 (1999).
- [18] E. K. Yuldashbaeva, J. Libert, P. Quentin, and M. Girod, *Phys. Lett. B* **461**, 1 (1999).
- [19] L. Próhniak, P. Quentin, D. Samsøen, and J. Libert, *Nucl. Phys. A* **730**, 59 (2004).
- [20] T. Nikšić, Z. P. Li, D. Vretenar, L. Próhniak, J. Meng, and P. Ring, *Phys. Rev. C* **79**, 034303 (2009).
- [21] Z. P. Li, T. Nikšić, D. Vretenar, J. Meng, G. A. Lalazissis, and P. Ring, *Phys. Rev. C* **79**, 054301 (2009).
- [22] Z. P. Li, B. Y. Song, J. M. Yao, D. Vretenar, and J. Meng, *Phys. Lett. B* **726**, 866 (2013).
- [23] D. R. Inglis, *Phys. Rev.* **103**, 1786 (1956).
- [24] R. Beck, H. J. Mang, and P. Ring, *Z. Phys.* **231**, 26 (1970).
- [25] J. L. Egidio and L. M. Robledo, *Phys. Rev. Lett.* **70**, 2876 (1993).
- [26] W. Satua and R. A. Wyss, *Rep. Prog. Phys.* **68**, 131 (2005).
- [27] W. Koepf and P. Ring, *Nucl. Phys. A* **493**, 61 (1989).
- [28] W. Koepf and P. Ring, *Nucl. Phys. A* **511**, 279 (1990).
- [29] A. V. Afanasjev, J. König, and P. Ring, *Phys. Rev. C* **60**, 051303R (1999).
- [30] H. Madokoro, J. Meng, M. Matsuzaki, and S. Yamaji, *Phys. Rev. C* **62**, 061301(R) (2000).
- [31] J. Peng, J. Meng, P. Ring, and S. Q. Zhang, *Phys. Rev. C* **78**, 024313 (2008).
- [32] P. W. Zhao, S. Q. Zhang, J. Peng, H. Z. Liang, P. Ring, and J. Meng, *Phys. Lett. B* **699**, 181 (2011).
- [33] P. W. Zhao, S. Q. Zhang, and J. Meng, *Phys. Rev. C* **92**, 034319 (2015).
- [34] J. Meng, J. Peng, S. Q. Zhang, and P. W. Zhao, *Front. Phys.* **8**, 55 (2013).
- [35] P. W. Zhao, J. Peng, H. Z. Liang, P. Ring, and J. Meng, *Phys. Rev. Lett.* **107**, 122501 (2011).
- [36] P. W. Zhao, J. Peng, H. Z. Liang, P. Ring, and J. Meng, *Phys. Rev. C* **85**, 054310 (2012).
- [37] P. Olbratowski, J. Dobaczewski, J. Dudek, and W. Plóciennik, *Phys. Rev. Lett.* **93**, 052501 (2004).
- [38] P. Olbratowski, J. Dobaczewski, and J. Dudek, *Phys. Rev. C* **73**, 054308 (2006).
- [39] I. Hamamoto, *Nucl. Phys. A* **271**, 15 (1976).
- [40] K. Hara, A. Hayashi, and P. Ring, *Nucl. Phys. A* **385**, 14 (1982).
- [41] J. L. Egidio, M. Borrajo, and T. R. Rodríguez, *Phys. Rev. Lett.* **116**, 052502 (2016).
- [42] K. Hara and Y. Sun, *Int. J. Mod. Phys. E* **4**, 637 (1995).
- [43] Y. Sun, Y.-C. Yang, H.-L. Liu, K. Kaneko, M. Hasegawa, and T. Mizusaki, *Phys. Rev. C* **80**, 054306 (2009).
- [44] Y. Yang, Y. Sun, K. Kaneko, and M. Hasegawa, *Phys. Rev. C* **82**, 031304 (2010).
- [45] P. Ring, *Prog. Part. Nucl. Phys.* **37**, 193 (1996).
- [46] D. Vretenar, A. V. Afanasjev, G. A. Lalazissis, and P. Ring, *Phys. Rep.* **409**, 101 (2005).
- [47] J. Meng, H. Toki, S. G. Zhou, S. Q. Zhang, W. H. Long, and L. S. Geng, *Prog. Part. Nucl. Phys.* **57**, 470 (2006).
- [48] P. Ring, in *Relativistic Density Functional for Nuclear Structure*, Vol. 10, edited by J. Meng (World Scientific, Singapore, 2016) Chap. 1, pp. 1–20.
- [49] H. Kucharek and P. Ring, *Z. Phys. A* **339**, 23 (1991).
- [50] P. W. Zhao, Z. P. Li, J. M. Yao, and J. Meng, *Phys. Rev. C* **82**, 054319 (2010).
- [51] P. Ring and P. Schuck, *The Nuclear Many-Body Problem* (Springer-Verlag, Berlin, 1980).
- [52] J. Daoutidis and P. Ring, *Phys. Rev. C* **80**, 024309 (2009).
- [53] J. M. Yao, H. Mei, H. Chen, J. Meng, P. Ring, and D. Vretenar, *Phys. Rev. C* **83**, 014308 (2011).
- [54] Y. K. Gambhir, P. Ring, and A. Thimet, *Ann. Phys. (N.Y.)* **198**, 132 (1990).
- [55] T. Nikšić, N. Paar, D. Vretenar, and P. Ring, *Comp. Phys. Comm.* **185**, 1808 (2014).
- [56] B. Pritychenko, M. Birch, B. Singh, and M. Horoi, *At. Data Nucl. Data Tables* **107**, 1 (2016).
- [57] I. Daoutidis and P. Ring, *Phys. Rev. C* **83**, 044303 (2011).
- [58] T. Bürvenich, D. G. Madland, J. A. Maruhn, and P.-G. Reinhard, *Phys. Rev. C* **65**, 044308 (2002).
- [59] T. Nikšić, D. Vretenar, and P. Ring, *Phys. Rev. C* **78**, 034318 (2008).

- [60] M. Devlin, D. R. LaFosse, F. Lerma, D. Rudolph, D. G. Sarantites, and P. G. Thirolf, Phys. Rev. C **61**, 017301 (1999).
- [61] L. Liu and P. Zhao, Sci. China Phys. Mech. Astron. **55**, 2420 (2012).
- [62] J. Egido, H.-J. Mang, and P. Ring, Nucl. Phys. A **334**, 1 (1980).